Macromolecules

Article

pubs.acs.org/Macromolecules

Effect of Long Chains on the Threshold Stresses for Flow-Induced Crystallization in iPP: Shish Kebabs vs Sausages

Lucia Fernandez-Ballester,[†] Derek W. Thurman,[‡] Weijun Zhou,[§] and Julia A. Kornfield*,[⊥]

[†]Department of Mechanical and Materials Engineering, University of Nebraska at Lincoln, Lincoln, Nebraska 68588, United States

[‡]Baytown Technology and Engineering Complex, ExxonMobil Chemical Co., 5200 Bayway Dr., Baytown, Texas 77520, United States

[§]Core R&D – Materials Science & Engineering, The Dow Chemical Company, 2301 N. Brazosport Blvd., B-1470, Freeport, Texas 77541, United States

[⊥]Division of Chemistry and Chemical Engineering, California Institute of Technology, Pasadena, California 91125, United States

ABSTRACT: The addition of small concentrations (2 wt % or less) of ultrahigh molecular weight isotactic polypropylene ($M_L \sim 3500$ kg/mol) to a matrix of lower molecular weight chains ($M_S \sim 186$ kg/mol, e.g. $M_L/M_S \sim 20$) substantially decreases the critical stress for inducing a highly oriented skin under flow-induced crystallization conditions—significantly more than for blends of $M_L/M_S \sim 5$ (Seki et al.)—and promotes the formation of point precursors and oriented "sausage-like" structures not observed for $M_L/M_S \sim 5$. These differences correlate with the onset of long chain stretching during shear: the ratio of long chains' Rouse time to short chains' disengagement time indicates that 3500 kg/mol chains can easily stretch if tethered onto a point nuclei and even when untethered. Adding 3500 kg/mol chains has strong effects that saturate beyond the overlap concentration, suggesting that an uninterrupted supply of long chains greatly accelerates formation of threads. A conceptual model is proposed that distinguishes between a critical stress for shish initiation and that for propagation.

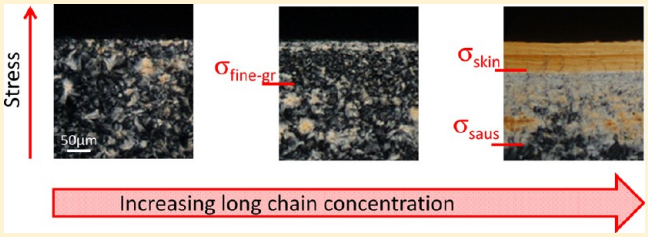

1. INTRODUCTION

Renewed interest in flow-induced crystallization (FIC) of polymers has been fueled by a combination of innovative experimental methods,[1−7] advances in control of molecular variables,[8−12] and discoveries that challenge long-standing concepts.[13−16] Technologically, processing flows can greatly accelerate the kinetics of crystallization and induce the formation of highly oriented solid-state morphologies that have very different properties from quiescently crystallized material of identical molecular composition: the highly oriented morphology confers greater density, modulus, and hardness and lower permeability and thermal expansion coefficient.[17−24] The different crystallization environments in a flow field can produce a "skin-core" morphology that has dense, oriented crystalline layers and an isotropic crystalline core, with a relatively sharp boundary between them.[1,20,21,25] Thus, the effects of flow are so highly nonlinear that there seem to be "thresholds" that, once crossed, lead to qualitatively different behavior. An array of controlling variables have been proposed over the years, i.e., melt entropy, shear stress, shear rate, strain, and specific work.[4,6,23,25−29] However, it is not yet known how to best define such thresholds or how they depend on the molecular attributes of the polymer.

Phenomenologically, for a given material, there is evidence of a threshold stress σ_{pt} above which shear flow can induce the formation of "point-like" nuclei[a] and below which shearing has negligible effect. Another critical shear stress $\sigma_{skin} > \sigma_{pt}$ is associated with the ability of shear to induce prolific formation of oriented "thread-like" precursors, also known as "shish". Thread-like precursors provide nucleating surfaces from which oriented lamellae—also known as "kebabs"—grow radially. When the separation between shish is so small that cyllindrulites impinge prior to significant noncrystallographic branching a highly oriented morphology results, known as the "highly oriented skin". There is evidence that the presence of point nuclei is a prerequisite for prolific formation of shish,[1,28,31,32] but the exact nature and mechanisms of formation of both point-like and thread-like precursors remains the subject of debate. Proposed mechanisms of formation of shish include propagation upstream and downstream from already present point-like precursor,[1] the aggregation or accumulation of point-like nuclei,[28] and stretching of segments of chains tethered by junctions in an entangled physical network.[33,34]

To gain further insight into the formation of thread-like precursors (a.k.a. shish), this study examines the molecular basis of the effects of "long chains". The longest chains in the melt strongly influence the formation of shish,[13,27,35−42] and it is thought that their ability to undergo significant degrees of orientation or stretch during flow is key to their effects.[43−45] In contrast, the creation of point-like nuclei is insensitive to long chains, suggesting that the average segmental orientation

Received: January 5, 2012
Revised: June 2, 2012
Published: August 1, 2012

   dx.doi.org/10.1021/ma3000384 | *Macromolecules* 2012, 45, 6557−6570

dominates this process.[27] Efforts to establish the specific roles of the length and concentration of long chains studying the formation of shish include a number of studies using the bimodal blend approach.[4,13,26,27,33,46−48] The specific design of a model blend determines the type of information that can be extracted regarding the mechanism of formation of flow-induced precursors.

Here, bimodal blends with long chains that are unusually large compared to the matrix chains ($M_L/M_S \sim 20$) are used to explore the effect of chain stretching. To draw conclusions regarding the effect of long chain length, the matrix polymer is the same as in our previous study that examined $M_L/M_S \sim 5$ using long chains of 923K g/mol (referred to here as 1M).[27] The constituent polymers have fairly narrow distribution, rather than components with broad distributions.[26,33,47,49] Shish in the highly oriented skin are not solely composed of long chains,[14] so we use a matrix polymer that crystallizes as readily as the long chains, rather than acting as a solvent.[46,47] The concentration of long chains is kept low ($C_L \leq 2$ wt %), so all of the blends in the present study and in our prior study with 1M long chains have nearly matched quiescent crystallization kinetics and morphology; thus, comparisons at a specific temperature represent *well-matched subcooling*. The small concentrations of long chains also give all the blends viscosity similar to that of the matrix alone (within a factor of 3); thus, comparisons made at a specific shear stress for a specific shearing time represent *approximately matched rates of deformation, melt entropy, total strain, and specific work*.[4,23,26,28,50,51] Therefore, the present blends enable us to unambiguously identify effects due to long chains. The results indicate that the onset of chain stretching in the longest chains may govern the formation of oriented thread-like precursors.[45] We propose a conceptual model that is consistent with the observed effects of long chain length and concentration on the processes of initiation and propagation of thread-like precursors.

2. EXPERIMENTAL SECTION

Bimodal blends of isotactic polypropylene (iPP) were prepared with low concentrations (2 wt % or less) of high molecular weight (M_w = 3500K g/mol, M_w/M_n = 1.8, referred to as 3.5M "long chains") chains in a matrix of shorter, yet still highly entangled chains (M_w = 186K g/mol, M_w/M_n = 2.3, "Base-PP"), where M_w and M_n are the weight-average and number-average molecular weights. Both polymers, provided by Dow Chemical Co., were synthesized using metallocene catalysts (Table 1). The "long" polypropylene has somewhat greater stereoregularity ([mmmm] > 98%) than the short chains ([mmmm] = 96%).

The "Base-PP" is the same resin used in a previous bimodal blend study by Seki et al.[27] The 3.5M long chains were synthesized as follows: A 2 L stainless steel reactor was charged with triethylaluminum (1 mL, 1M) as a scavenger, purified liquid propylene (600 g), and a metallocene catalyst (0.105 g). The catalyst was rinsed in hexane (10 mL) twice and was allowed to prepolymerize at 20 °C for 10 min. The reactor was then slowly heated to 70 °C over a period of ∼12 min, and the reaction was left to run at 70 °C and 470 psi pressure for a total of 70 min. The product was flash transferred into a knockout drum and transferred into a vacuum oven for drying.

Because of the vastly different molecular weights of the two iPPs, bidisperse materials were prepared by solution blending, as described previously.[6,27] Briefly, desired amounts of 3.5M "long chains" and Base-PP (Table 2) were dissolved in hot xylene under an inert atmosphere until a homogeneous solution was obtained and then quickly precipitated into cold methanol. The resulting "fluff" was filtered and washed with methanol and then sprayed with a measured amount of an acetone solution of a 1:1 mixture of antioxidants (Irganox 1010 and Irgafos 168) to achieve 2000 ppm to the polypropylene. Finally, the polymer fluff was dried at 80 °C under vacuum for several days to ensure removal of all remaining solvent. As a control, Base-PP (no 3500K long chains added) was subjected to the same solution blending procedure (B0). Long chain concentrations C_L up to ∼5 times their overlap concentration (C_L*) were examined (Table 2):

$$C_L^* = \frac{3M_w}{4\pi(R_g^2)^{3/2}N_a} \quad (1)$$

where R_g is the radius of gyration and N_a is Avogadro's number. Using the literature value of $(\langle R_g^2\rangle)^{1/2}/(M_w^{1/2}) = 0.39$ Å/(g/mol)$^{1/2}$,[52] long chains of 3500 kg/mol long chains have $C_L^* = 0.0036$ g/cm^3. The blends were characterized by differential scanning calorimetry (DSC) using a Perkin-Elmer DSC-7 instrument with 6−9 mg of sample under a N_2 atmosphere. Peak temperatures during the second heating and cooling cycle between 220 and 50 °C at a rate of 5 °C/min are reported as T_m and T_x, respectively (Table 2).

Flow-induced crystallization experiments were carried out in an apparatus[2] capable of imposing a strong shear pulse on a polymer melt for a precisely controlled time and prescribed thermal conditions. The flow channel consists of a rectangular slit with aspect ratio >10:1.[2] The maximum strain that can be applied to the polymer melt is constrained by the geometry of the channel, as described in the Supporting Information of Kumaraswamy et al.[13] We use pressure-driven slit flow because it allows quick imposition and removal of very high wall shear stresses. This experimental configuration has a trade-off in that the stress is not uniform, which must be taken into account when interpreting the depth-averaged observables recorded in real time, i.e., birefringence, turbidity, and wide-angle X-ray diffracted intensity.[6] In the velocity gradient direction, the imposed shear stress varies linearly from the value at the wall (σ_w) to 0 at the center of the flow channel (Figure 1). The experimental protocol (Figure 2) was as follows: the flow cell was filled with the polymer melt using a low wall shear stress at 215 °C; it was held at this temperature (T_{erase}) for 5 min to erase any history effects and to fully relax the melt;[27] then the melt was cooled to T_x (137 °C), and a brief shear pulse with a specified wall

Table 1. Molecular Characteristics of the Isotactic Polypropylene Components Used for the Bimodal Blends

	M_w (kg/mol)[a]	M_n (kg/mol)[a]	M_w/M_n	[mmmm] (mol %)[b]	T_m (°C)[c]
Base-PP	186.0	86.9	2.3	96.0	149.3
3.5M	3500	1950	1.8	>98	144.3

[a]Determined by GPC-MALLS. [b]^{13}C NMR. [c]The apparent melting temperature was determined as the peak temperature of differential scanning calorimetry (DSC) endotherm on second heating with scanning rate of 5 °C/min under a N_2 atmosphere.

Table 2. Characteristics of the Bimodal Blends of 3.5M Long Chains in Base-PP Short Chains[a]

	3.5M (wt %)	C_L (mg/cm^3)	C_L/C_L*	T_x (°C)	T_m (°C)
B0	0	0	0	109.9	149.6
0125p	0.125	1.07	0.3	111.3	151.1
025p	0.25	2.14	0.6	110.9	150.2
05p	0.5	4.27	1.2	110.6	150.5
1p	1	8.54	2.4	110.8	149.6
2p	2	17.08	4.8	110.8	149.6

[a]C_L is the concentration of 3.5M long chains. T_x and T_m were determined as the peak temperatures of differential scanning calorimetry (DSC) traces on second cooling and heating, respectively. The scanning rate was 5°C/min, and measurements were performed under a N_2 atmosphere.

dx.doi.org/10.1021/ma3000384 | Macromolecules 2012, 45, 6557−6570

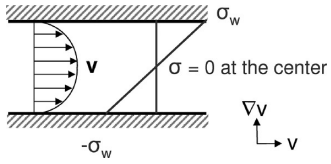

Figure 1. Schematic showing flow profile and shear stress profile across the gap of the rectangular slit channel. The *in-situ* optical and *ex-situ* X-ray beam traverse the sample along the velocity gradient direction, denoted ∇**v**.

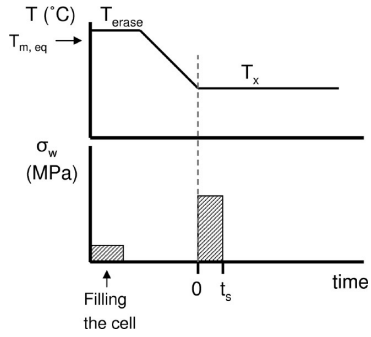

Figure 2. Experimental protocol for flow-induced crystallization experiments.

shear stress (σ_w) was imposed for a specific shearing time (t_s). Subsequently, the progress of isothermal crystallization at 137 °C was monitored with rheo-optical methods for 75 min; then the flow cell was removed from the apparatus and allowed to cool to room temperature over ∼10 min. The sample was then removed for *ex-situ* characterization. Control experiments under quiescent conditions (in which no shear pulse is imposed) were performed, and two sets of *ex-situ* samples were prepared: one set was cooled after 75 min of isothermal crystallization for comparison with the shear experiments above, and the other set was given 14 h to crystallize isothermally to visualize the quiescent nucleation density at 137 °C.

Real-time optical measurements probe the optical anisotropy and degree of turbidity of the polymer sample during and after shear, as described elsewhere.[2] The laser beam traverses the flow channel in the velocity gradient direction ∇**v** (Figure 1). The incoming beam is linearly polarized at 45° with respect to **v**; the transmitted light is analyzed using a polarizing beamsplitter so that the intensities transmitted through crossed and parallel polarizers are recorded simultaneously ($I_\perp$ and $I_\parallel$, respectively). At early times (when the retardance $\delta < \pi$), δ is computed using eq 2. At later times ($\delta > \pi$), the retardance is estimated from the successive maxima (and minima) in the $I_\perp/(I_\perp + I_\parallel)$ signal, corresponding to integer orders, $n\pi$.[53] Prior to the onset of significant depolarization due to multiple scattering, $I_\perp/(I_\perp + I_\parallel)$ can be used to evaluate the retardance:

$$\frac{I_\perp}{I_\perp + I_\parallel} = \sin^2\left(\frac{\pi \Delta n d}{\lambda}\right) = \sin^2\left(\frac{\delta}{2}\right) \quad (2)$$

where Δn is the birefringence, d is the length of the optical path through the sample, λ is the wavelength of the probing beam, and δ is the retardance. The turbidity of the sample is monitored by normalizing the total intensity of the beam transmitted through the sample at a given time by the initial intensity that was transmitted through the melt before shear was imposed:

$$\frac{I_{total}(t)}{(I_{total})_0} = \frac{I_\perp + I_\parallel}{(I_\perp + I_\parallel)_0} \quad (3)$$

Ex-situ characterization of the final morphology was performed using polarized optical microscopy (POM) and wide-angle X-ray diffraction (WAXD). Optical micrographs of sections cut in the flow-velocity gradient plane (**v**–∇**v**) were recorded through crossed polarizer (P) and analyzer (A) using two orientations of the sample: with the flow direction parallel or at 45° with respect to P. Two-dimensional WAXD patterns of selected quenched samples were recorded with the X-ray beam oriented along the ∇**v** direction (the same direction as the laser beam during real-time rheo-optical measurements). WAXD measurements were performed on the X27C beamline of the U.S. National Synchrotron Light Source (NSLS at Brookhaven National Laboratory, Upton, NY) using X-ray wavelength of 1.371 Å. Patterns were recorded with a MAR CCD detector placed 17 cm from the sample. The camera length was calibrated with an Al_2O_3 standard. The 2D WAXD patterns were normalized by the beam intensity; the intensity due to background was subtracted. The azimuthal dependence of the scattered intensity was computed for the reflection corresponding to the (110) plane of the α crystal morph of isotactic polypropylene.

3. RESULTS

Quiescent Crystallization. The addition of small concentrations (up to 2 wt %) of 3.5M long chains to the base resin Base-PP did not change the kinetics of quiescent crystallization as indicated by DSC measurements under nonisothermal conditions (Table 2) and by turbidity during isothermal quiescent crystallization at 137 °C (Figure 3). Nor did the

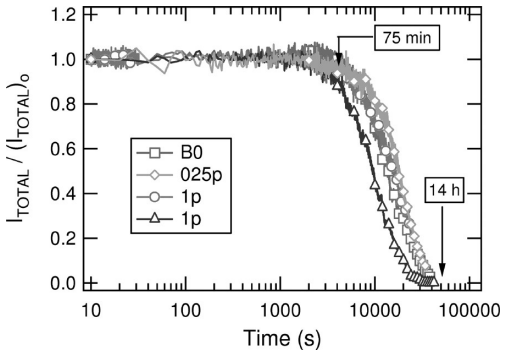

Figure 3. *In-situ* turbidity measurement during quiescent crystallization at 137 °C of B0, 025p, and 1p. Results for duplicate experiments on 1p are shown (circles and triangles) to illustrate variability due to the small number of nucleation events that occur in the sample volume. Arrows indicate the time points at which samples were cooled to ambient temperature and removed for *ex-situ* evaluation.

added long chains discernibly affect the morphology formed during quiescent, isothermal crystallization at 137 °C for 14 h (Figure 4, left and middle micrographs). *Ex-situ* micrographs show a small number of large spherulites (up to 200 μm in diameter) for both B0 and 1p. The difference between the pair of duplicate 1p experiments shown in Figure 3 illustrates that quiescent crystallization times determined by turbidity can vary up to 50% due to the small number of nucleation events that occur at 137 °C in the volume probed by the laser beam. Note that very little turbidity develops during the first 75 min, the time at which sheared specimens are cooled. For comparison to the micrographs of the sheared samples, quiescent experiments were also performed using the same hold time (75 min at 137 °C): the resulting quiescent morphology has much smaller spherullites than the case of 14 h at T_x followed by cooling (Figure 4, compare right vs center micrographs).

Effect of C_L on Flow-Induced Morphologies. In contrast to quiescent crystallization, the addition of long chains strongly affects the final morphology obtained when shear is imposed on the subcooled melt. To isolate the effects of C_L specifically, the

dx.doi.org/10.1021/ma3000384 | *Macromolecules* 2012, 45, 6557–6570

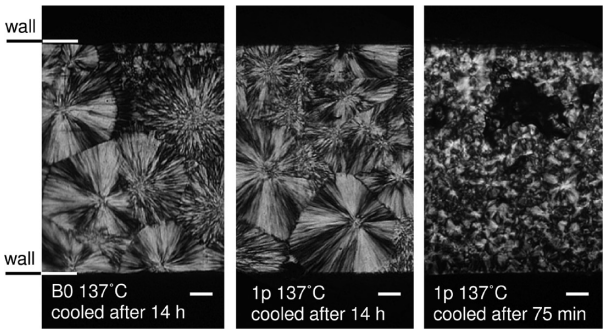

Figure 4. Polarized optical micrographs of the *ex-situ* morphology after quiescent crystallization at 137 °C of B0 cooled after 14 h (left), 1p cooled after 14 h (center), and 1p cooled after 75 min (right). The 14 h holding time at 137 °C was chosen such that spherullites grow to impingement isothermally and nucleation during cooling can be neglected. Nonisothermal nucleation and growth play a major role in determining the morphology when cooling begins after 75 min. Note that there is no evidence of enhanced nucleation at the wall. Scale bars correspond to 50 μm.

behavior of the different binary blends are compared at a fixed T_x = 137 °C, total mass extruded (~100 mg), and isothermal hold time (75 min) prior to cooling to ambient temperature for specific choices of the wall shear stress σ_w.

The base resin B0 did not form a highly oriented skin even for the high wall shear stress of σ_w = 0.11 MPa (Figure 5 top), while the addition of 0.25 wt % of 3.5M chains was sufficient to enable formation of oriented precursors (highly oriented skin for 025p in Figure 5, bottom). However, both B0 and 025p exhibited a fine-grained layer—a macroscopically isotropic region with smaller structures—and a spherullitic core, with the

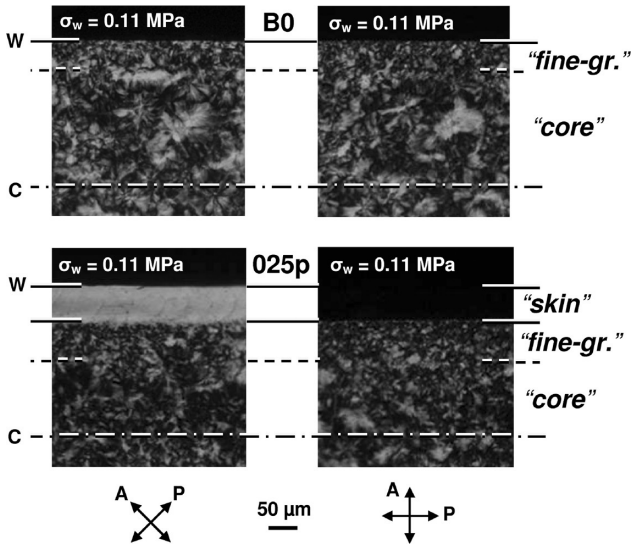

Figure 5. *Ex-situ* polarized optical micrographs for B0 (top) and 025p (bottom) crystallized at 137 °C for 75 min after imposing a pulse of σ_w = 0.11 MPa, then cooled, removed, and sectioned. To impose similar total shear strain at the wall, shearing times were chosen to give matched extruded amounts of ~100 mg (t_s = 1.4 and 2.4 s for B0 and 025p, respectively). Flow direction is horizontal. Left column: polarizer P is 45° to flow; right column: P is parallel to flow. The distance between the center (C) and the wall (W) is 250 μm. The lines at the margin of the figures indicate the threshold stresses for flow-induced formation of (solid line) a highly oriented skin and (dashed line) a fine grained layer (values shown in Figure 8).

fine-grained layer extending a greater distance from the wall in 025p than for B0.

When the wall shear stress is reduced to an intermediate level, σ_w = 0.065 MPa, the sample with C_L = 0.25 wt % (025p, Figure 6 middle) only develops a very thin irregular layer

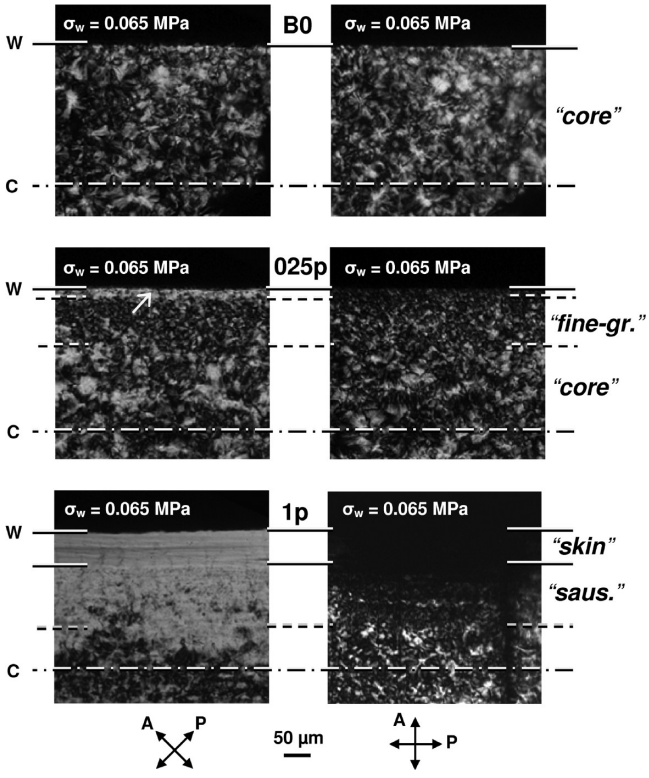

Figure 6. *Ex-situ* polarized optical micrographs of B0 (top), 0.25p (middle), and 1p (bottom) sheared at 137 °C with wall shear stress σ_w = 0.065 MPa and cooled after 75 min. The arrow (middle, left) points to a structure that appears bright for polarizer P and analyzer A at ±45° with respect to the flow direction and dark when P and A are parallel and orthogonal to the flow direction. The extruded amounts were ~100 mg (t_s = 8.3, 8.7, and 12 s for B0, 025p, and 1p, respectively).

having a few oriented structures near the wall that appear bright when P/A are at ±45° to flow (left). In contrast, the blend with C_L = 1 wt % (1p) develops a highly oriented skin that is ~60 μm thick (Figure 6, bottom), has a narrow spherulitic core region near the center of the channel, and has an irregular, birefringent region from approximately 60 to 160 μm from the wall with many oriented "sausage-like" structures (shish-kebab structures in which the oriented lamellae have grown to great distances from the central thread), called the "sausage layer". The highly oriented skin is much more birefringent and uniform than the "sausage" layer. This distinction is easily observed when P is placed along the flow direction (right image): the skin area is completely dark, while the sausage morphology shows bright and dark striated structures. Note that neither B0 nor 025p exhibits a region significantly populated with sausage-like structures.

Increasing C_L further enabled oriented morphologies to form at progressively reduced shear stress: while σ_w = 0.065 MPa was sufficient to induce a highly oriented skin for C_L =1 wt % (but not for 0.25 wt %), Figure 6, a lower σ_w = 0.037 MPa induced

dx.doi.org/10.1021/ma3000384 | Macromolecules 2012, 45, 6557–6570

both a sausage layer and a thick, highly oriented skin in the 2 wt % blend 2p (but not a highly oriented skin in 1p), Figure 7.

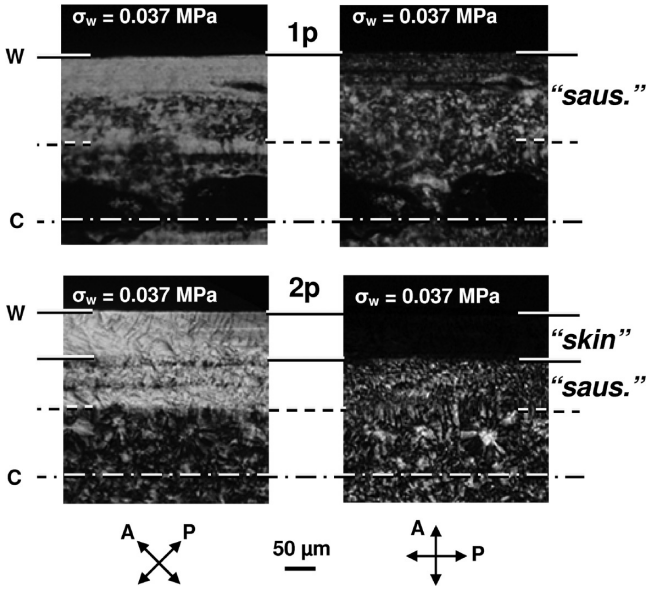

Figure 7. *Ex-situ* polarized optical micrographs for 1p (top) and 2p (bottom) crystallized at 137 °C for 75 min after imposing a pulse of σ_w = 0.037 MPa. Extruded amounts were ~100 mg (t_s = 26 and 27 s for 1p and 2p, respectively).

In general, as σ_w increased, the boundaries between morphological layers for a given C_L shifted farther from the wall (Figure 7 to Figure 5), consistent with a particular shear stress, denoted σ_i, where i denotes the type of boundary.[b] The boundary of the highly oriented skin is generally sharp and uniform, allowing the stress at the boundary to be evaluated fairly precisely, which revealed that the boundary of the oriented skin coincided with a specific value of the shear stress. As C_L increases, this "threshold stress" σ_{skin} decreases. The boundary between the unoriented core and the adjacent layer (either the sausage layer or the fine-grained layer) is more diffuse and variable. Nevertheless, these boundaries also shifted in a manner consistent with a threshold stress and yielded values of $\sigma_{fine\text{-}gr}$ or σ_{saus}. Interestingly, samples showed either a fine-grained layer (if C_L < 0.5 wt %) or a "sausage" layer (if C_L ≥ 0.5 wt %), but not both (e.g., Figure 6 bottom).[c]

The threshold shear stress to induce the highly oriented skin morphology (σ_{skin}) decreases strongly as the concentration of long chains C_L increases from 0 to the overlap concentration C_L* (Figure 8, top graph). Even the addition of just 0.125 wt % of 3.5M long chains (corresponding to 0.3C_L*) reduces σ_{skin}. In contrast, for concentration of long chains $C_L > C_L$*, the effect of additional long chains on σ_{skin} is weak. The threshold stresses to induce a fine-grained morphology $\sigma_{fine\text{-}gr}$ or to induce a sausage layer σ_{saus} show a dependence with C_L similar to that of σ_{skin}. In the concentration range in which a fine-grained layer is observed (i.e., C_L/C_L* < 1.2), $\sigma_{fine\text{-}gr}$ decreases like σ_{skin} with the addition of long chains. Likewise, in the concentration range in which a sausage layer is observed (C_L/C_L* ≥ 1.2), the weak variation of σ_{skin} with C_L for is also observed in σ_{saus}.

The magnitude of the reduction in σ_{skin} for 3.5M long chains is much greater than that observed previously for 1M long chains (Figure 8, bottom) in the same base resin (Base-PP) subjected to the same flow-induced crystallization conditions as

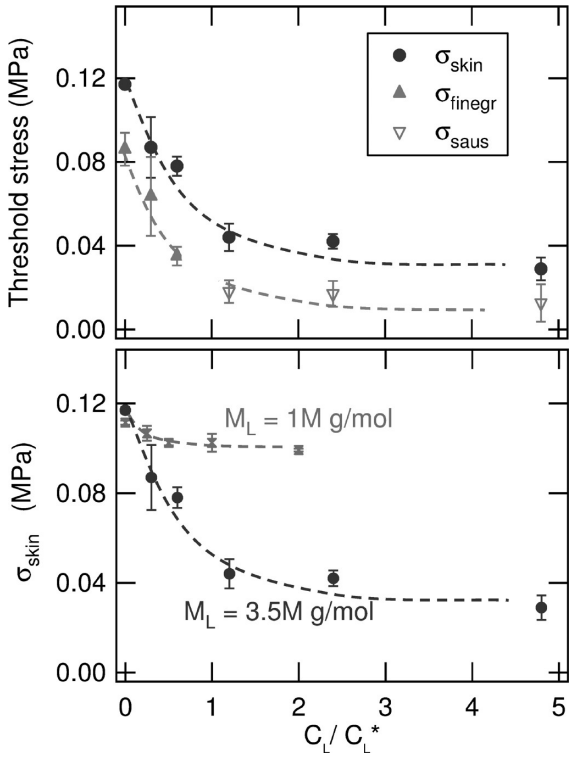

Figure 8. Top: effect of the concentration of 3.5M long chains C_L (relative to their overlap concentration C_L*) on σ_{skin} (for all C_Ls), on $\sigma_{fine\text{-}gr}$ (for the smaller C_Ls), and on σ_{saus} (for the bigger C_Ls) at 137 °C and fixed total mass extruded. The dashed curves are for guiding the eye. Error bars refer to variations in the thicknesses of the skin, fine-grained, and sausage areas. Bottom: comparison of the impact of M_L (either 1M from earlier studies[27,54] or 3.5M in the current study) of the long chains on σ_{skin}. C_L* is 0.0069 and 0.0036 g/cm^3 for 1M and 3.5M chains, respectively. The stresses reported in Seki et al.[27] were corrected according to Thurman.[54]

this study.[27,54] For both 1M and 3.5M most of the reduction of σ_{skin} occurs at low concentrations of long chains; the influence of C_L on σ_{skin} is weak at $C_L \geq 0.5C_L$* for 1M and at $C_L \geq 1.2C_L$* for 3.5M. Interestingly, both of these threshold concentrations correspond to similar volume fractions of long chains (0.4% for 1M and 0.5% for 3.5M).

The final solid-state structure in quenched specimens was characterized using *ex-situ* wide-angle X-ray diffraction with the beam along the ∇v direction, averaging over the various morphologies present in a given sample (Figure 1). These depth-averaged patterns are interpreted by building on previous microfocus X-ray patterns obtained for each different type of morphology[6] and by comparing pairs of samples that only differ in the presence or absence of a given type of morphology. The diffraction patterns showed predominantly the α crystal morph of iPP. Weak reflections of the γ-morph were observed; no sign of the β-morph was found. The (110) reflection of the α-iPP crystal morph provides information about both the oriented parent lamellae (with c-axis along the flow direction) and their epitaxial daughter lamellae (at approximately ±80°). For the lowest wall shear stress (σ_w = 0.037 MPa), the azimuthal distribution of the (110) intensity (Figure 9 top) shows strong orientation only for 2p (in accord with its thick highly oriented skin, Figure 7 bottom); the milder orientation seen in 1p correlates with the presence of a "sausage" layer, but without a highly oriented skin (Figure 7 top). The parent-to-daughter

dx.doi.org/10.1021/ma3000384 | Macromolecules 2012, 45, 6557−6570

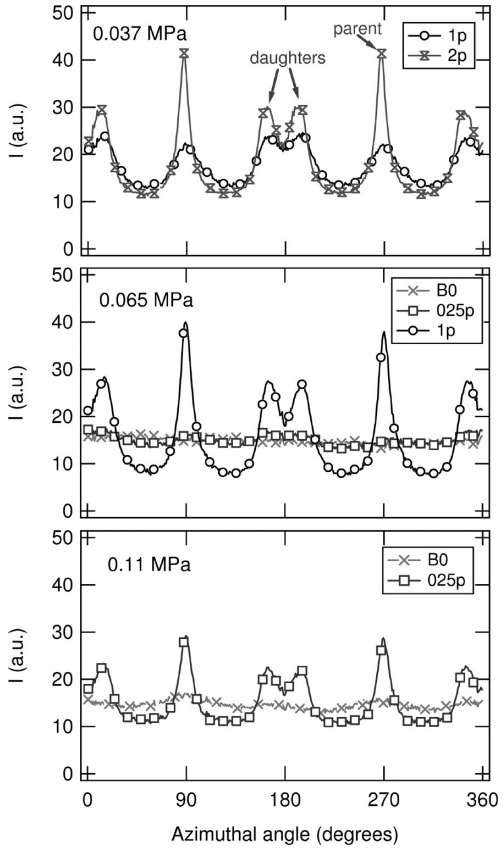

Figure 9. *Ex-situ* WAXD azimuthal distribution of the (110) reflection of α-iPP. Samples were sheared at 137 °C and σ_w = 0.037 MPa (top), 0.065 MPa (center), and 0.11 MPa (bottom), and they were cooled and extracted after 75 min of isothermal crystallization. They correspond to the polarized optical micrographs shown in the previous figures: compare top to Figure 7, center to Figure 6, and bottom to Figure 5.

ratio is significantly greater for the 2p sample than for 1p, as expected for a highly oriented skin.[6,55] The next higher stress (σ_w = 0.065 MPa, Figure 9 center) induces a very high degree of orientation in 1p, accompanied by a relatively high ratio of parent-to-daughter peaks (consistent with the oriented skin, Figure 6, bottom), whereas both B0 and 025p show an approximately isotropic orientation distribution (in accord with spherulitic morphologies, Figure 6, top and middle). The highest wall shear stress (σ_w = 0.11 MPa, Figure 9 bottom) induces significant orientation even in 025p (in accord with its oriented skin, Figure 5 bottom); however, B0 remains approximately isotropic (consistent with its spherulitic morphology, Figure 5 top).

Development of Semicrystalline Morphology *in Situ*. The kinetic processes leading to the observed effects of long chains on the final solid-state morphology are revealed by the development of crystallization during and after imposition of the shear pulse. During short-term shearing at the lowest wall shear stress applied, σ_w = 0.037 MPa, only 2p developed a birefringence upturn (inset, Figure 10a): after the first 20 s of shearing, when the melt contribution dominates (nearly the same for 1p and 2p), the birefringence of the 2p sample increases strongly in a manner characteristic of formation of thread-like precursors and oriented crystallites (kebabs) on them.[25] Upon cessation of flow, only a small fraction of the retardance of the 2p sample relaxes (similar in magnitude to the drop in birefringence for 1p). After the rapid relaxation, the birefringence of both 1p and 2p continues to increase, indicating growth of oriented crystals. For sample 2p (which exhibits both a highly oriented skin and a sausage layer in *ex-situ* micrographs, Figure 7 bottom), the retardance increased rapidly, reaching a half-wave in ~60 s (Figure 10a). In contrast, the retardance of 1p (which in the *ex-situ* micrographs shows a sausage layer but no highly oriented skin, Figure 7 top) increased very slowly: at the time the retardance of 2p reached a full wave (ca. 130 s), the retardance of 1p was only 0.02—roughly 1/30th that of 2p. Even for this modest imposed stress, the time scale over which the samples became turbid ($t_{1/2}$ ~ 300 s, Figure 10b) was reduced by at least an order of magnitude relative to quiescent crystallization ($t_{1/2}$ ~ 10 000 s in Figure 3). Interestingly, the 2p transmitted intensity decays in two steps, while the transmittance for 1p decays monotonically (see Discussion section).

Increasing the wall shear stress to σ_w = 0.065 MPa at the same mass extruded, T_x, and isothermal hold time (~100 mg, 137 °C, 75 min, as above) induces prolific formation of oriented thread-like precursors in 1p manifested by the birefringence upturn during the shear pulse, which did not fully relax after flow was stopped (Figure 10c). The formation of thread-like precursors in 1p accords with the highly oriented morphologies observed *ex situ* by POM (Figure 6 bottom) and WAXD (Figure 9, middle). Growth of oriented crystallites (kebabs) in 1p was manifested by an increase of retardance after cessation of flow. Neither B0 nor 025p exhibits a birefringence upturn, in accord with the absence of a highly oriented skin (Figure 6, top and middle). The sample that formed an oriented skin (1p) showed a two-step decay of the transmitted intensity (an early drop followed by a plateau, then a decay to zero, Figure 10d), while the samples with weak orientation (both 025p and B0) showed a monotonic decay. In all cases the samples became turbid much sooner than in the quiescent experiments (compare Figure 10d to Figure 3, note difference in scale).

Finally, the highest stress (σ_w = 0.11 MPa, with the same mass extruded, T_x, and isothermal hold time as above) induced a highly oriented skin in 025p, but not in B0 (Figure 5 and Figure 9 bottom). During the shear pulse, the *in-situ* birefringence initially rises to the same value for both 025p and B0 (Figure 10e, inset), which corresponds to the melt flow birefringence (hence, average segmental orientation). A subsequent upturn in the birefringence is observed for 025p, but not for B0, and after cessation of flow, the birefringence only partially relaxes for 025p, and soon after it grows strongly (Figure 10e). The birefringence upturn during shear and the long-lived birefringence after shear are known to be signatures of prolific formation of oriented precursors which give rise to the highly oriented skin.[25] In contrast, the birefringence completely decays for B0 after flow is stopped and does not significantly increase before the end of the experiment. The time scales for decay of transmittance (Figure 10f) are much faster than under quiescent conditions for both B0 and 025p; however, the shape of the decay is "two-step" for 025p and monotonic for B0.

For the experiments that exhibited an upturn in birefringence during flow, the time elapsed between the inception of shear and the appearance of the upturn (t_u) was estimated using the intersection of the steady-state melt flow birefringence and a line through the early upturn in birefringence. This procedure was feasible because the present bimodal blend behaved like

dx.doi.org/10.1021/ma3000384 | *Macromolecules* 2012, 45, 6557–6570

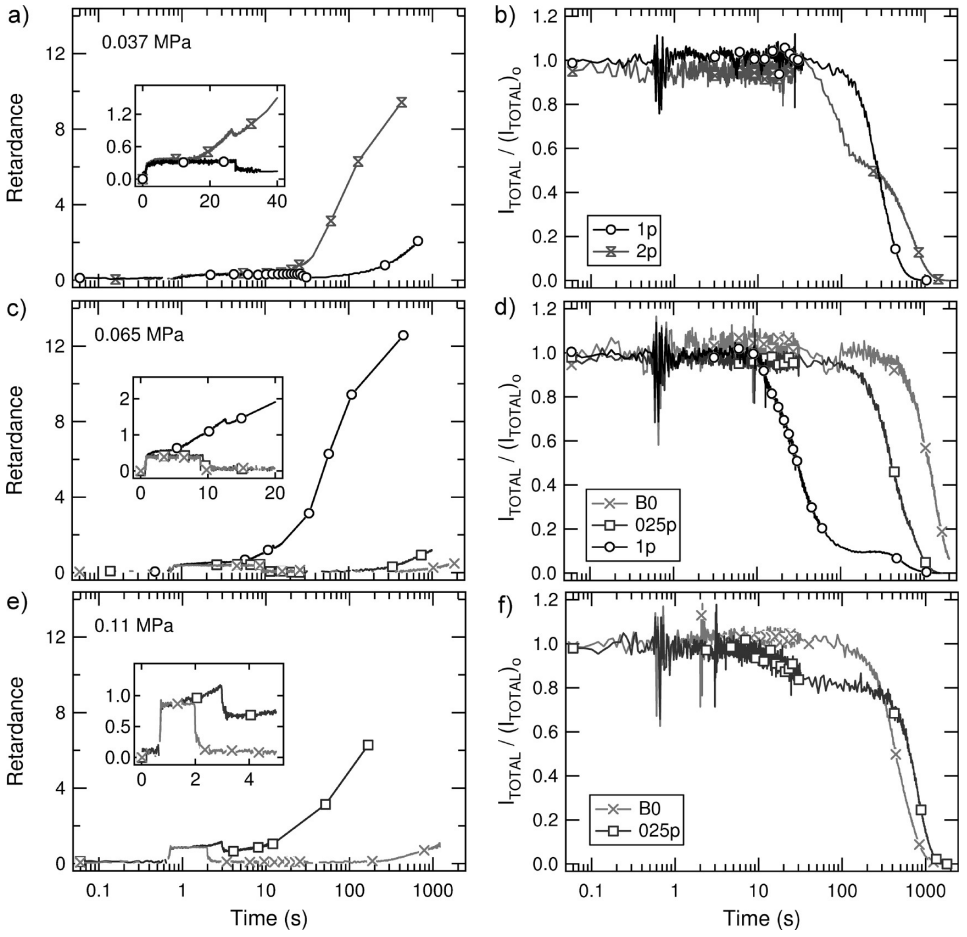

Figure 10. Real-time optical retardance (left) and turbidity (right) measurements for different blends subjected to flow-induced crystallization at 137 °C and different σ_w. (a, b) 1p and 2p subjected to σ_w = 0.037 MPa and t_s = 26 and 27 s, respectively. (c, d) B0, 025p, and 1p subjected to σ_w = 0.065 MPa and t_s = 8.3, 8.7, and 12 s, respectively. (e, f) B0 and 025p subjected to σ_w = 0.11 MPa and t_s = 1.4 and 2.4 s, respectively. Extruded mass was ∼100 mg. Insets in left column show the details of the birefringence upturn during and right after shear.

those of Seki et al. in that an overshoot in melt birefringence did not occur upon inception of shear, which facilitated the determination of upturn times even when they were small in magnitude.[27] In contrast, Ziegler−Natta polypropylenes typically exhibit a birefringence overshoot upon inception of shearing before reaching a plateau value.[2,3]

The "upturn time" t_u for the blends decreases strongly as σ_w increases at each concentration of long chains (Figure 11). For a fixed wall shear stress and 3.5M long chains, t_u initially decreases with increasing C_L (for $C_L/C_L^* \leq 1.2$), then becomes insensitive to C_L at higher concentrations ($C_L/C_L^* \geq 1.2$). Interestingly, $C_L/C_L^* = 1.2$ is also the concentration of 3.5M long chains at which σ_{skin} became insensitive to C_L (Figure 8). This saturation behavior is in accord with the steady value of t_u observed for the 1M bimodal blends of Seki et al., where all three C_L that showed an upturn belonged to the range where the effect of 1M long chains had already saturated (Figure 11).[27,54]

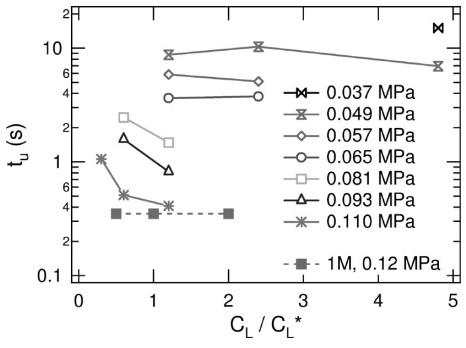

Figure 11. Time for upturn (t_u) in birefringence signal during the shear pulse at 137 °C for different wall shear stresses and C_Ls of 3.5M long chains. The data on 1M long chains and 0.12 MPa from Seki et al. are also plotted.

4. DISCUSSION

To examine the changes in behavior associated with the transition from long-chain orientation to long-chain stretching, the present series of binary blends is designed such that the ratio of the long-chain Rouse time to the short-chain disengagement time, $\tau_{R,L}/\tau_{D,S}$, largely determines whether or not the long chains undergo chain stretching. The blends all have zero shear viscosity close to that of the pure short chains, specifically $\eta_{blend} \in (\eta_S, 3\eta_S)$. Therefore, all of the blends can be viewed as having viscosity that scales with the product of the plateau modulus of iPP G_N° and the short-chain disengagement time $\tau_{D,S}$ (empty square on the timeline in Figure 12): $\eta_S \approx \tau_{D,S} G_N^\circ$. Thus, for a given applied shear stress σ, the resulting shear rate scales as $\sim\sigma/(\tau_{D,S} G_N^\circ)$. Consequently, chain stretching of long chains is expected when $\sigma/(\tau_{D,S} G_N^\circ) > (1/$

dx.doi.org/10.1021/ma3000384 | Macromolecules 2012, 45, 6557−6570

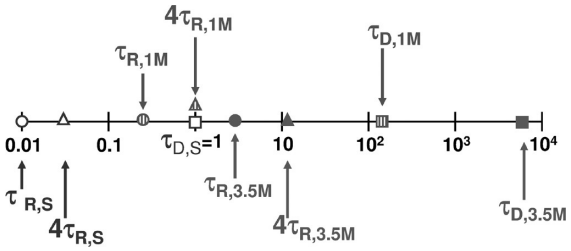

Figure 12. Retraction times for untethered and tethered short chain ($\tau_{R,S}$, $4\tau_{R,S}$), 1M long chains ($\tau_{R,1M}$, $4\tau_{R,1M}$), and 3.5M long chains ($\tau_{R,3.5M}$, $4\tau_{R,3.5M}$) relative to the short chain disengagement time, $\tau_{D,S}$. Reptation times of 1M and 3.5M are also indicated ($\tau_{D,1M}$ and $\tau_{D,3.5M}$).

$\tau_{R,L}$) or, equivalently, when $\tau_{R,L}/\tau_{D,S} > G_N^\circ/\sigma$. Here, we examine a range of shear stresses that corresponds to G_N°/σ from 4 to 10. Long chains of 3.5M provide $\tau_{R,L}/\tau_{D,S} \approx 3$, such that the highest stress imposed in this study approaches the transition from long-chain orientation to long-chain stretching. To our knowledge, this is the first set of experiments in which the deformation rate reaches the threshold for chain stretching for long chains of well-defined length and concentration.

In addition to the relaxation dynamics of free chains in the bulk, the dynamics of chains attached to a precursor may be important in the physics at the ends of a rapidly propagating shish. Under conditions that induce a highly oriented skin, shish can increase in length at a rate on the order of 10 μm/s;[d] thus, successive ordering events near a propagating tip occur orders of magnitude faster than in the rest of the melt. Perhaps the relative ease of stretching of a tethered long chain contributes to the rapid ordering that occurs near a propagating tip. The chain length equilibration time of a grafted chain may be estimated using a simple argument. A tethered chain of a given length has Rouse modes equivalent to a free chain of twice that length. Since the Rouse time τ_R varies quadratically with chain length, a dangling strand with most of the length of the free chain will have roughly 4-fold longer Rouse time ($4\tau_R$) than a free chain of the same length.

Effect of M_L/M_S on Long Chain Stretching. The stronger decrease of σ_{skin} upon addition of 3.5M long chains than for 1M long chains (Figure 8 bottom) can be ascribed to the onset of long chain stretching as M_L/M_S increases. Free long chains of 1M g/mol are unlikely to undergo stretching ($\tau_{R,1M} < \tau_{D,S}$: compare striped circle to open square in Figure 12), based on

$$\tau_{R,L} = \frac{N_e}{3N_S}\left(\frac{N_L}{N_S}\right)^2 \tau_{D,S} \quad (4)$$

where N_e is the number of monomers in an entanglement strand, and N_S, N_L are the number of monomers in a short and a long chain, respectively.[56] Only for an end-adsorbed 1M g/mol long chain would stretching be plausible ($4\tau_{R,1M} \approx \tau_{D,S}$, striped triangle and open square, Figure 12). Increasing the length of the long chains to 3.5M g/mol opens the possibility of chain stretching in the bulk ($\tau_{R,3.5M} > \tau_{D,S}$: compare filled circle to open square in Figure 12), and adsorbed 3.5M long chains would be expected to experience chain stretching ($4\tau_{R,3.5M} > 10\tau_{D,S}$, filled triangle vs open square in Figure 12).

Two Types of Oriented Morphologies. In contrast to binary blends using 1M long chains, two types of oriented regions form in the 3.5M bimodal blends—a highly oriented skin and regions populated with "sausage-like" structures. Both the highly oriented skin and the sausage layer develop from oriented thread-like precursors—although with very different concentrations (Figure 13). The highly oriented skin is

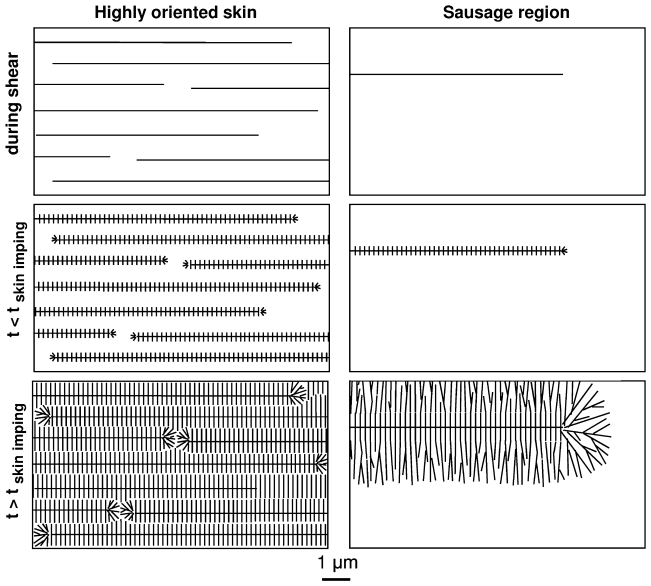

Figure 13. Schematic of formation and development of highly oriented skin (left column) and sausage region (right column). Top: shear produces a much higher concentration of thread-like precursors in the skin than in the sausage region. Middle: after cessation of flow (but before impingement of skin) oriented lamellae (i.e., kebabs) grow off the thread-like precursors. Bottom: in the skin, oriented lamellae impinge with one another at short times (due to small interdistances), while in the sausage region, oriented lamellae continue to grow off the central thread and are able to undergo noncrystallographic branching and splaying at farther distance, decreasing their degree of orientation.

templated by long threads that are *closely spaced* (submicrometer spacing between the shish).[1,27,57] Indeed, electron micrographs of the highly oriented skin have shown >1 (μm of shish)/(μm^3).[25] In contrast, the distances between sausages—and therefore, between the threads running down their middle—are typically on the order of ~10 μm or more (large enough to be observed by optical microscopy, Figure 6 bottom, Figure 7, Figure 14). Therefore, we can estimate that the order of magnitude of shish concentration is ~0.01 (μm of shish)/(μm^3) or less in the sausage layer.

The substantial difference in concentration of threads between the "sausage layer" and the highly oriented skin is evident in real-time measures of structure formation during and after short-term shear. First, the upturn in birefringence during shear, which correlates with subsequent formation of a highly oriented skin (insets of Figure 10a,c,e[3,25]), was absent when

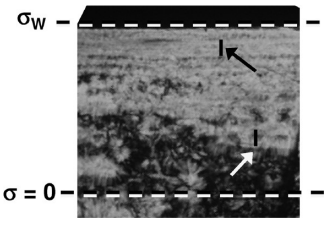

Figure 14. Polarized optical micrographs of 1p sheared at 137 °C with σ_W = 0.044 MPa below σ^*_{skin} but above σ^*_{saus} showing typical region populated with sausages. The vertical black lines have a length of 25 μm and encompass approximately 2−3 sausages.

dx.doi.org/10.1021/ma3000384 | Macromolecules 2012, 45, 6557−6570

only sausages formed (inset of Figure 10a). Evidently, the thread-like precursors in the sausage layer are dilute: their birefringence and any due to kebabs grown during shear is negligible relative to the melt flow birefringence (Figure 13 top, compare left vs right). Second, after cessation of shear, the rate of oriented crystallization is vastly lower when only sausage layers form than when an oriented skin forms[6] (Figure 10a,c,e). After the melt relaxes, growth of kebabs occurs with the linear growth rate typical of quiescent crystallization,[58] which is—by design—the same for all samples in the present study. Therefore, the slower oriented crystallization in the sausage layer unambiguously indicates that it has a much lower concentration of shish than the oriented skin (Figure 13 middle, compare left vs right). Third, the small and relatively uniform distances between threads in the highly oriented skin—but not in the "sausage layer"—lead to relatively short impingement times, evidenced by an abrupt decrease in the rate of oriented crystallization[57] and a plateau or even an increase of transmittance[3,59] (compare Figure 15a–c vs Figure 15d). For example, impingement at ~100 s corresponds to a distance of ~1 μm between shish in the highly oriented skin (based on the linear growth rate of $G \sim 0.003$ μm/s for a similar iPP at 137C[60]). In contrast, sausage layers do not show signs of impingement *in situ* because the distance between oriented precursors is much greater than the distance a growth front can advance before turbidity precludes further optical measurements (Figure 13 bottom, compare left vs right). For example, after shearing 1p at $\sigma_w = 0.037$ MPa, the distance between oriented precursors is ~20 μm (Figure 7 top left), which is much greater than the ~1.5 μm distance the growth front can advance before the sample becomes turbid (~400 s, Figure 10b). Thus, there is a clear distinction between the highly oriented skin and the sausage layer.

The significantly different concentrations of shish in the highly oriented skin and the sausage layer are consistent with the degree of orientation observed in the final solid state, which is much greater in samples that have a highly oriented skin than those with only sausage layers (Figure 9, top). In the highly oriented skin, impingement occurs at relatively short times and at small distances from the shish where oriented lamellae are laterally constrained, and therefore, all their growth occurs with a high degree of orientation (Figure 13, bottom left). In contrast, in the sausage layer lamellae are able to grow farther from their central shish, giving them more time and space to undergo noncrystallographic branching and splaying, thus decreasing their orientation correlation (Figure 13, bottom right). In addition, spherulitic structures interdispersed between the sausage structures arise due to point nuclei formed during shear and due to the nonisothermal formation of point-like nuclei during cooling (illustrated in Figure 4, right). These interdispersed spherulitic structures further contribute to the lower degree of orientation of the fully solidified sausage layer.

Interestingly, the boundary between the sausage region and the highly oriented skin is rather sharp: A discontinuity in birefringence is evident at the boundary, even for samples with a relatively high concentration of sausages near the highly oriented skin (Figure 6 bottom, Figure 7 bottom). This suggests that for our 3.5M blends there is a qualitative change in the ability to prolifically create high concentrations of thread-like precursors at σ_{skin}—not a gradual transition—which inspires the conceptual model proposed below.

Conceptual Model for Formation of Thread-like Precursors. In the following, we extend an earlier conceptual model[27] to explain the role of the long chains in formation of thread-like precursors, building upon the idea that shish form in the flow direction starting from point-like nuclei. Prolific formation of thread-like nuclei does not occur until after a significant number of point-nuclei have formed during shear flow, suggesting that their presence is necessary.[1,28,31,32,61] Beyond that point, the process of shish formation is still the subject of debate. An often-stated mechanism is the aggregation of extended long chains;[38,62] but recent experimental results showing that thread precursors are not enriched in long chains disfavor this mechanism.[14] Another hypothesis suggests that formation of shish results from the coalescence of point nuclei once their number becomes sufficiently large.[28] However, point precursors are typically several micrometers apart,[e] and the diffusivity of multichain aggregates is expected to be slower than that of individual molecules. Thus, it is difficult to devise a

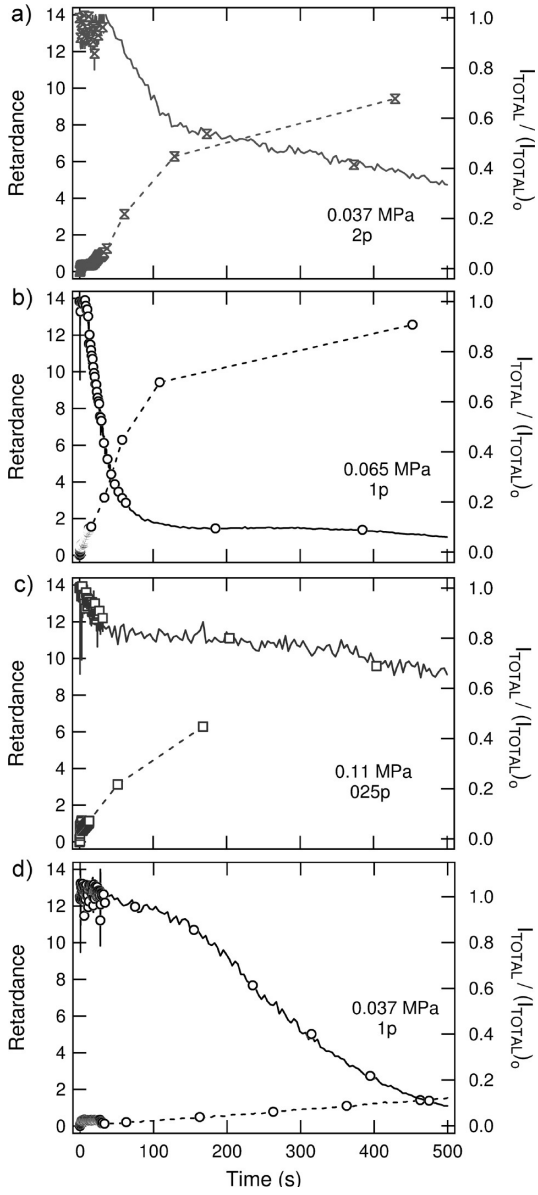

Figure 15. Impingement signatures in retardance (dashed trace) and turbidity (solid trace) at 137 °C for samples that develop a highly oriented skin (a) 2p at $\sigma_w = 0.037$ MPa, (b) 1p at $\sigma_w = 0.065$ MPa, and (c) 025p at $\sigma_w = 0.11$ MPa vs sample that only develops sausage region (d) 1p at $\sigma_w = 0.037$ MPa.

dx.doi.org/10.1021/ma3000384 | *Macromolecules* 2012, 45, 6557–6570

mechanism that could bring a sufficient number of point-like nuclei together and position them into a line fast enough to produce ~10 μm of shish per second. Instead, the morphologies generated by shearing (fine grained, sausage, and highly oriented skin) suggest that special conditions are created immediately upstream (or downstream) of a previously formed precursor. For this reason, we build upon a proposed mechanism that treats formation of thread-like precursors as a quasi-stationary process in which growth propagates upstream and downstream from the primary point-like nuclei; i.e., the thread-like precursor grows in length from its tips.[1,27]

Nanoscopic regions near an existing thread-like precursor locally support a much higher rate of ordering events than the rest of the sheared melt—by orders of magnitude. The local rate of ordering events at a propagating tip can be approximated from the propagation velocity (~10 μm s^{-1}) of a shish. If shish increase in length by ordering events immediately adjacent to the tip (i.e., within a distance of R_g of a short chain, ~10 nm[f]), an upper bound of the local rate of transforming melt into ordered structure corresponds to one ordering event per $(10\ nm)^3$ per ms, i.e., ~10^9 $\mu m^{-3} s^{-1}$. A *lower bound* can be obtained by speculating that ordering at distances up to ~100 nm from the propagating tip can add to the growing shish (on the order of the R_g of a 3.5M long chain or perhaps by a sequence of physically associated chains): ~10^6 μm^{-3} s^{-1}. For comparison, the rate of formation of point-like precursors in the bulk of the melt can be estimated from the distance between point nuclei in fine-grained layers, i.e., ~10 μm apart; thus, point-like precursor formation occurs at rates less than one event per $(10\ \mu m)^3$ per s (i.e., ~10^{-3} μm^{-3} s^{-1}). A generous upper bound on this bulk ordering rate can be obtained by speculating that only 1-in-1000 precursors go on to become active nuclei: ~10° μm^{-3} s^{-1}. Even with a conservative bound on the local rate of ordering events at a growing tip and a generous bound on the rate of ordering events in the melt as a whole, they *differ by 6 orders of magnitude*. Because of this, we focus on the physical processes that might occur locally, very near point-like nuclei—but not in the bulk of the melt.

To account for the formation of both the sausage region and the highly oriented skin, we distinguish two different processes in the development of a thread from a point-like precursor: initiation and propagation. *Initiation* of threads must occur profusely at the high stresses ($\sigma > \sigma_{skin}$) that produce high concentrations of shish. On the basis of the sharp boundary of the highly oriented skin, we consider physics that may explain a threshold stress for prolific initiation of threads. *Propagation* is essential to the formation of long threads, whether closely spaced or far apart. The morphology of the sausage layer indicates that the shish can propagate to great lengths (tens of micrometers) at stresses that can be much lower than the threshold for prolific initiation ($\sigma_{saus} \sim {}^1/_2\sigma_{skin}$). The present model accounts for both a threshold stress σ_{init} to activate a point-like precursor into a propagating thread and a lower threshold stress to propagate shish σ_{prop}. After describing the conceptual model, we show that it also accounts for the observed effects of M_L (1M vs 3.5M long chains) and of C_L on σ_{skin} and σ_{saus}.

Initiation of a Thread. The longest molecules in the melt are known to play a particularly important role in formation of thread-like precursors, and it is known that they access greater-than-average degrees of orientation or stretch relative to the matrix of shorter chains.[45] However, we have seen above that the degree of orientation or stretch of the long chains in the bulk melt only explains ordering events at a rate of ~10° μm^{-3} s^{-1} or less—not sufficient to generate shish. Therefore, like Seki et al.,[27] we consider the *local* increase of orientation that may result from the adsorption of a long chain on a point-like nucleus during shear (Figure 16a,b). (Short chains also adsorb, but their relaxation is so rapid that, even when tethered, they do not stretch, Figure 12.) Adsorption requires either diffusive or convective transport of the chain to the surface of the point-nuclei. If shearing continues after a long chain attaches to a point-like precursor, portions of the chain can be convected away from the nucleus, producing a "streamer" that emanates from the point-like nucleus.[27] Tension in the segments of the long chain close to the tethering point induces a local level of orientation and stretch that is not found elsewhere in the melt (Figure 16c); thus, a characteristic length ξ of a tethered long chain will have particularly high segmental orientation, while segments near the free end are only slightly perturbed. If ξ is of the same order as R_g of the long chains, then 3.5M chains might have ξ of ~100 nm. Neighboring chains that are not themselves stretched are influenced by the enhanced orientation and stretch of the ξ-section(s) of long chain(s) that are tethered to the precursor. Thus, the conditions generated immediately upstream and downstream of a precursor are exceptional, providing a plausible explanation for a local enhancement of the rate of ordering events by orders of magnitude (perhaps ~10^6 μm^{-3} s^{-1}) that initiates thread formation (Figure 16d).

In this physical picture, the length of the long chains is expected to have a very strong effect. Increasing M_L results in both stronger orientation of the chain segments near the tether point (due to the greater "drag force" on the dangling long chain) and longer "reach" of the ξ portion in which significant

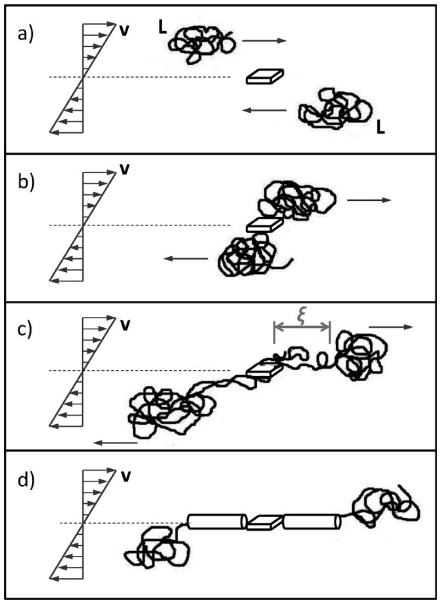

Figure 16. Schematic of initiation of thread-like precursors. Relative velocity profile is shown on the left. The dashed line indicates the streamline of an already present point nuclei—not the center of the channel. Only long chains are shown (short chains that are also present, able to adsorb and are incorporated into the thread are omitted). Long chains are convected toward a point nuclei (a) and adsorb onto it (b). A characteristic length "ξ" near the tethering point develops a local high level of orientation and stretch (c) that promotes a local enhancement of ordering events, thus initiating the thread (d).

dx.doi.org/10.1021/ma3000384 | *Macromolecules* 2012, 45, 6557–6570

stretching occurs (Figure 16c). Thus, the present conceptual model could explain the decrease in the threshold stress for thread initiation, σ_{init} observed with increasing M_L/M_S.

This physical picture is also compatible with the nonlinear effects of long-chain concentration C_L, particularly as it approaches long-chain overlap C_L^*. Elsewhere in the melt it is very unlikely that two long chains simultaneously have stretched portions in proximity to each other. In contrast, adsorption of two (or more) long chains to a given point-like precursor provides spatiotemporal correlation of stretched segments. As C_L increases, the probability that two or more long chains attach to the same point precursor increases. In turn, increasing the number of long chain "streamers" attached to a given precursor would, at a given stress, increase the average orientation in the volume in which the "ξ portions" overlap. Consequently, the stress required to produce the threshold level of segmental orientation (within a distance ξ of the precursor) to initiate propagation, σ_{init}, would initially decrease as C_L increases. Experimentally, it is observed that the effect of increasing C_L becomes weak beyond the long-chain overlap concentration (e.g., for $C_L > 1.2C_L^*$ in Figure 8). When C_L reaches C_L^*, a long chain is almost always in the vicinity of the precursor; perhaps that is sufficient to saturate the capacity of the precursor for adsorption, possibly explaining the mild effect of C_L on σ_{init} once it is greater than C_L^*.

Propagating a Thread. After a shish has been initiated from a point nucleus, its further propagation is facilitated by the existence of the "ξ portions". Propagation of shish must involve successive attachments of long chains to the tips of the growing shish, since many long chains are involved in the formation of a typical shish. Shish are typically much longer than the reach of a single chain, making it impossible to explain shish formation with just one or even a few long chains.[g] Under conditions that produce a highly oriented skin, long chains are present in the shish at a concentration that matches their concentration in the surrounding melt,[14] suggesting that at least one long chain per ~100 nm of shish is involved in the process of forming that shish. Although the precise nature of the propagating front is not known, we consider two different ways that long chains might play a role: long chains might adsorb to the shish as they are convected past (as suggested above for initiation, Figure 17a) or a shish might incorporate long chains in its path by overtaking them (Figure 17b, an additional mechanism enabled by the "ξ portions"). Thus, the long chains required to maintain the propagating front may be supplied by incorporation or adsorption or both. When this occurs, new streamers with a stretched portion ξ form and the propagation process continues.

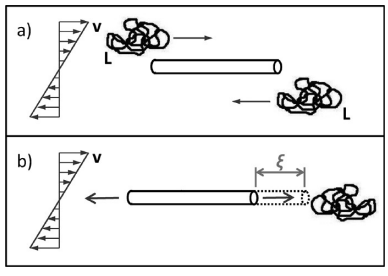

Figure 17. Schematic of propagation of thread precursors. The growth front can propagate (a) via adsorption of convected long chains or (b) by interception of long chains by the propagating tip.

Propagation is expected to be sensitive to the probability of finding another long chain within a distance ξ of the propagating tip. When $C_L < C_L^*$, a long chain may not be available near the tip of the shish. On one hand, if the length ξ (Figure 16c) spans the characteristic center-to-center distance between dilute long chains, the thread is likely to "intercept" a long chain. The newly added long chain will extend a streamer on the order of ~ξ and "catch" another long chain, resulting in a quasi-stationary process. Propagation by interception would thus depend strongly on the relative magnitude of C_L and of the reach of ξ (which increases with increasing M_L and σ). On the other hand, adsorption of a long chain that is flowing past the tip is limited by the average time required for a long chain to arrive at the propagating tip, which depends on the distance between long chains and their relative velocity with respect to the tip ($\sim R_{g,L} \times$ [shear rate]). The probability of adsorption events also increases with increasing C_L, σ, and M_L. Therefore, for $C_L < C_L^*$, there is an interplay between C_L, M_L/M_S, and σ that determines whether or not propagation will occur and how rapidly it will advance. Once C_L^* has been reached, finding a long chain nearby should be relatively easy, so further increase of long chain concentration may have a weak effect on propagation. Overall, this physical picture suggests that the required stress for propagation σ_{prop} may be less than σ_{init} due to the ξ-portions that are present after the initiation step.

Physical Significance of the Boundary between Sausages and Skin. The conceptual model above can capture the existence of two distinct oriented morphologies: both regions satisfy the condition for propagation of a thread, but only the highly oriented skin satisfies the condition for prolific "initiation". The dilute threads characteristic of sausage regions suggest that they form at stresses below σ_{init}, where very few of the point-like precursors convert to propagating shish. We speculate that in the neighborhood of particles (e.g., catalyst fragments, dust) the stress could exceed σ_{init}. The formation of sausages depends strongly on C_L: they are most evident near and above C_L^* for 3.5M chains in binary blends that readily propagate long shish, suggesting that once a relatively infrequent event starts the shish, the propagation continues relatively easily if $C_L > C_L^*$ (i.e., $\sigma_{init} > \sigma_{prop}$).

How Long Is "Long" Enough? The comparison of the present binary blends with 3.5M g/mol long chains and our earlier work in the same base resin with ~1M g/mol long chains shows qualitatively different effects. While 1M long chains reduce σ_{skin}, the effects are much weaker than those seen with 3.5M long chains (Figure 8 bottom). This suggests that 1M long chains are just at the threshold length required to influence the transition to oriented growth in a matrix of 186K iPP. Even if tethered at its end, the 1M long chain has a Rouse time comparable to the reptation time of the matrix, which controls the shear rate in the present experiments ($4\tau_{R,1M} \approx \tau_S$, Figure 12). Consequently, the 1M long chains might require a much higher stress to develop an appreciable stretched ξ-portion, while an adsorbed 3.5M chain ($4\tau_{R,3.5M} > 10\tau_S$) may undergo facile formation of a stretched ξ-portion. In turn, this may explain why the addition of as little as $0.3C_L^*$ has a strong effect for 3.5M, while very weak changes in flow-induced crystallization were seen at $0.25C_L^*$ for 1M.

The absence of a sausage layer in the case of M_L = 1M may be further evidence that it is a borderline case, indicating that $\sigma_{skin} \approx \sigma_{saus}$ (equivalently $\sigma_{init} \approx \sigma_{prop}$). In contrast, the more pronounced ξ-portion of tethered 3.5M chains (Figure 16c) gives them greater reach, which would facilitate addition of long

dx.doi.org/10.1021/ma3000384 | Macromolecules 2012, 45, 6557−6570

chains by incorporation—thus reducing the threshold stress for propagation relative to that for initiation. If the 1M chains do represent a marginal case, the criterion $4\tau_{R,L^*} \approx \tau_S$ may provide a useful estimate of the minimum M_L/M_S required (in a matrix with reptation time τ_S) for a small concentration of long chains to significantly modify initiation and propagation of shish.

How Many Long Chains Are Enough? As noted earlier,[27] the dramatic enhancement of shish formation by long chains is not a single chain effect. The nonlinear decrease of σ_{skin} as concentration C_L increases to C_L^* (Figure 8 top) is explained in the conceptual model by the nonlinear effect of having two or more long chains attached to a precursor, thus reducing the macroscopic stress σ required to create sufficient local orientation to initiate or propagate a shish. If it were a single chain effect, at any given stress σ, the rate of initiation and propagation of threads would simply increase in proportion to C_L and the threshold stresses would not change significantly. In contrast, at a stress of $\sigma_w = 0.065$ MPa, the effect of long chains qualitatively changes as C_L increases 4-fold from $0.6C_L^*$ to $2.4C_L^*$ (025p to 1p, Figure 6), which cannot be explained by a simple 4-fold increase in the rate of processes active in the $C_L = 0.6C_L^*$ material.

It is important to note that the collaborative effect of long chains in the conceptual model does not require long chain-long chain entanglements, particularly for the $C_L \leq C_L^*$ blends where the strong nonlinear effects of concentration on σ_{skin} are observed. This is in contrast to studies where the formation of oriented structures is attributed to the increase in orientation or stretch caused by entanglements between the longest chains in the melt.[33,47,49,63] In our bimodal blends, no significant degree of long chain-long chain entanglement is expected even for the highest C_L. Furthermore, once the long chains pervade the entire volume ($C_L \geq C_L^*$), the concentration effect on σ_{skin} becomes weaker—not stronger—for both M_L = 1M g/mol[27,54] and 3.5M g/mol (e.g., σ_{skin} varies weakly with increasing concentration beyond $C_L \approx C_L^*$, Figure 8 bottom). Within the context of our model, the saturation as C_L increases suggests that point-like precursors may have a limited capacity to adsorb long chains, which becomes saturated when long chains pervade the entire volume.

Time for Birefringence Upturn. During shear at sufficiently high stresses $\sigma \geq \sigma_{skin}$, the prolific formation of shish (and some kebabs)[6] can produce a sharp increase in birefringence. Thus, the "birefringence upturn time" t_u provides a measure of the time elapsed from inception of shear to prolific initiation of threads from which a highly oriented skin develops. Recent experimental results suggest that the time lag between inception of shear and prolific formation of shish may be mainly attributed to the time required to form flow-induced point-like precursors. For instance, Janeschitz-Kriegl and co-workers observed a steady increase in the number of point-like nuclei up to 10^{16} m^{-3} with increasing specific work and formation of shish at higher values of work.[28] Also, Housmans et al. deduced an increase in the number of point-nuclei with increasing shearing time up to a saturation value of 10^{14} m^{-3} before the emergence of shish.[32] In view of this, the reduction of the upturn time as C_L is increased (but still below C_L^*) for the 3.5M blends suggests that the addition of a few 3.5M chains perceptibly enhances the rate of formation of point-like precursors. Some evidence of this can be seen in Figure 6 middle: addition of just $0.6C_L^*$ (i.e., 0.25%) of 3.5M long chains leads to a fine-grained layer ~100 μm thick (where $\sigma >$ 0.4 MPa) in which spherulites are much smaller than the corresponding region in B0. If the upturn time is governed by the lag time for formation of point-like precursors, the insensitivity of t_u when $C_L > C_L^*$ may indicate a saturation of the effect of 3.5M chains on formation of point-like precursors.

In contrast to the 3.5M long chains, the addition of 1M long chains did not noticeably enhance the formation of point-like precursors in the same matrix polymer: the upturn time did not decrease and the spherulite size did not perceptibly change.[27] If point-like precursors are envisioned to form from isolated ordering events in the melt, the ability of long chains to undergo chain stretching ($\tau_{R,L} > \tau_S$) should play a role. As noted earlier, 1M chains in a 186K matrix do not satisfy this criterion ($\tau_{R,1M} < \tau_S$) chains, while 3.5M chains in the same matrix do have $\tau_{R,3.5M} > \tau_S$ (Figure 12, i.e., isolated untethered 3.5M chains can undergo chain stretching in the melt).

5. CONCLUSION

All long chains are not created equal. When placed into an identical matrix having molar mass $M_S \approx 27M_e$, a small concentration of chains having length $M_L/M_S \approx 20$ can have dramatically stronger effects than long chains with $M_L/M_S \approx 5$. At less than 0.2% by mass, long chains with $M_L/M_S \approx 20$ reduce the threshold stress for prolific shish formation by more than 30%—an effect that cannot be achieved with $M_L/M_S \approx 5$ even at the highest concentration examined (>1.5%). In addition, long chains of $M_L/M_S \approx 20$ have two effects that were not observed with $M_L/M_S \approx 5$: these very long chains enhance flow-induced formation of point-like precursors and flow-induced formation of "sausages". As suggested by Van Meerveld et al., these differences may relate to the extent of chain stretching of the long chains during shear.[45] Specifically, strong effects are observed for long chains whose Rouse time (required for chain length equilibration) is greater than the reptation time of the matrix chains ($\tau_{R,L} > \tau_{D,S}$). Note that this criterion depends not only on the ratio of chain lengths, M_L/M_S, but also on the degree of entanglement of the matrix, M_S/M_e: the condition $\tau_{R,L} > \tau_{D,S}$ is satisfied when $(M_L/M_S)^2 > 3M_S/M_e$. The more entangled the matrix, the greater the relative length of the long chains compared to the matrix chains must be to produce a dramatic enhancement in flow-induced crystallization.

By producing such strong effects on σ_{skin} (Figure 8), long chains with $M_L/M_S \approx 20$ unambiguously confirm three tentative conclusions based on $M_L/M_S \approx 5$. First, the mechanism by which long chains enhance shish formation is clearly cooperative: if it were a single chain effect, the threshold stress would not change with increasing C_L—for a particular short-term shear protocol, only the number of precursors formed would change and merely in proportion to C_L. Second, addition of long chains can enable prolific creation of thread-like precursors even at concentrations well below C_L^*. Third, the effect of further addition of long chains levels off above C_L^*, indicating that the supply of long chains in formation of shish is no longer a limiting factor.

Also, there appear to be two stages—initiation and propagation—in thread formation from an already present point-like nucleus, with initiation having a more stringent stress requirement than that required for propagation of the thread ($\sigma_{init} > \sigma_{prop}$). Thus, if an infrequent event—such as a locally higher stress in the vicinity of a dust particle or catalyst fragment—causes an initiation event at a lower stress than the critical stress for the skin, the thread may propagate for tens of micrometers if $\sigma > \sigma_{prop}$. This may explain the observation of

dx.doi.org/10.1021/ma3000384 | Macromolecules 2012, 45, 6557−6570

relatively long and isolated sausage-type structures in optical micrographs of this and other studies.[1,25,27]

In hindsight, prior experiments using long chains of 1M g/mol ($M_L/M_S \approx 5$) are now seen to be a marginal case: only when tethered near their ends would the 1M long chains experience chain stretching. By moving to significantly longer chains, it becomes possible for 3.5M chains adsorbed anywhere along their length to develop a strongly oriented portion near the adsorption site. Indeed, we believe this produces a dramatic increase in proliferation of shish. The data are consistent with the hypothesis that the interaction of long chains with the tip of a shish creates a local orientation that is not found elsewhere in the flowing melt. The results anticipate that a molecular perspective on chain dynamics both in the melt and when adsorbed to precursors may provide predictive models linking molecular weight distributions and flow conditions with the resulting kinetics and morphology of crystallization. In relation to the concept of a critical molecular weight M_L*,[38,64] the present results caution against lumping all $M_L > M_L$* together. As chain length increases beyond the marginal length, qualitative changes in their effects occur, underscoring the importance of studies with model materials: even subtle differences in the distribution of the longest chains can have a considerable impact on the type of morphology that forms.

Physical insight into the molecular processes that determine whether a highly oriented skin or a "sausage" layer forms is important because the final properties in the solid state depend on the morphology. It is well-known that optical, thermal, transport, and mechanical properties all depend strongly on the level of orientation. Therefore, we offer a conceptual model that captures the occurrence of both "sausage" regions and the highly oriented skin. The mechanisms are speculative, as they cannot be observed directly. Nevertheless, they may provide the underpinnings of theoretical models with testable predictions regarding the dependence of the threshold stresses, propagation velocity, and upturn time that can be subjected to experimental validation.

AUTHOR INFORMATION

Notes

The authors declare no competing financial interest.

ACKNOWLEDGMENTS

We thank Dr. Robert Sammler of Dow Chemical Company for kindly providing the matrix iPP materials used in this study. We are also grateful to Dr. Igors Sics and Dr. Lixia Rong of beamline X27C (NSLS) for assistance in X-ray experiments. The ITP workshop is acknowledged, including discussions with Tom McLeish and Scott Milner. Funding was provided by the National Science Foundation under Grant DMR-0505393.

ADDITIONAL NOTES

[a]Point-like nuclei do not necessarily have a point-like geometry. We agree with Janeschitz-Kriegl's view,[30] which considers that all flow-induced precursors are long and slender. The spherulitic morphology that arises from the so-called point-like nuclei is simply a consequence of the large distance between those precursors relative to their length. Figure 10a of ref 31 shows a transmission electron micrograph in which a spherulitic structure has emerged due to "point-like" precursors of short length compared to the distance between them.

[b]In pressure-driven flow through a slit, the shear stress varies linearly from σ_w at the wall to zero at the center (Figure 1). Thus, the shear stress corresponding to the boundary between different morphologies is proportional to the distance from the center of the channel.

[c]It should be noted that the sausage-like structures may be embedded within a fine-grained layer but that the presence of the former may hinder the observation of the latter. Blends containing ≥0.5 wt % of long chains (C_L/C_L* ≥ 1.2) generally had a thick sausage layer without a clear fine-grained layer, so only σ_{saus} is reported.

[d]This rate is estimated from the TEM of Seki and co-workers[27] where the sample B1 is sheared for t_s = 1.4 s and exhibits shish longer than 20 μm (field of view).

[e]The observed distance between point nuclei in fine grained layers is on the order of ∼10 μm after shearing for more than 1 s at 0.11 MPa (Figure 5). Janeschitz-Kriegl et al.[28] found an upper bound of 10^{16} point nuclei/m^3 at the transition to shish formation, consistent with ∼10 μm of point-nuclei interdistance. An even lower point-nuclei density of $\sim 10^{14}$/m^3 was calculated by Housmans et al.[32] corresponding to a larger point-nuclei interdistance. Kumaraswamy et al.[57] observed spherulitic structures which were several micrometers in size in the fine-grained layer near the boundary with highly oriented skin.

[f]The radius of gyration R_g for base-PP, 1M chains, and 3.5M chains are estimated to be ∼17, 39, and 73 nm from $R_g/(M_w^{0.5}) = 0.39$ Å/(g/mol)$^{1/2}$.[52]

[g]Seki et al.[27] observed thread lengths of at least 20 μm (limited by the image field of view) for their 1M g/mol blends. Since the Rouse time of 1M long chains is faster than the short chain disengagement time (Figure 12), 1M chains are not expected to stretch when free in the melt and are a borderline case if they become adsorbed onto a point nuclei, so that not a significant amount of stretch is foreseeable. Thus, we can make a generous upper bound estimation of the extent of reach of a single 1M chain by estimating the size of an entanglement blob (∼2.5 nm) and computing the length of the chain if all blobs were laid out in a line, i.e., ∼0.5 μm. Therefore, a long chain must attach to the initial point nucleus to initiate the thread and, after initiation, successive attachments of long chains must occur to propagate the thread to greater lengths. It is highly unlikely for the long chains to attain a fully extended conformation under our shear conditions, but as an upper bound the maximum end-to-end length of 1M/mol chains is estimated as $R_{max} = Nb \sim 7$ μm. For our 3500 kg/mol long chains, we observe that some sausage structures can attain lengths over 100 μm (Figure 14), so the central thread in those sausages even exceeds the fully extended reach of a long chain $R_{max} = Nb \sim 24$ μm.

REFERENCES

(1) Liedauer, S.; Eder, G.; Janeschitzkriegl, H.; Jerschow, P.; Geymayer, W.; Ingolic, E. *Int. Polym. Process.* **1993**, *8* (3), 236−244.
(2) Kumaraswamy, G.; Verma, R. K.; Kornfield, J. A. *Rev. Sci. Instrum.* **1999**, *70* (4), 2097−2104.
(3) Langouche, F. *Macromolecules* **2006**, *39* (7), 2568−2573.
(4) Mykhaylyk, O. O.; Chambon, P.; Graham, R. S.; Fairclough, J. P. A.; Olmsted, P. D.; Ryan, A. J. *Macromolecules* **2008**, *41* (6), 1901−1904.
(5) Cavallo, D.; Azzurri, F.; Balzano, L.; Funari, S. S.; Alfonso, G. C. *Macromolecules* **2010**, *43* (22), 9394−9400.
(6) Fernandez-Ballester, L.; Thurman, D. W.; Kornfield, J. A. *J. Rheol.* **2009**, *53* (5), 1229−1254.

(7) Fernandez-Ballester, L.; Gough, T.; Meneau, F.; Bras, W.; Ania, F.; Francisco, J. C.; Kornfield, J. A. *J. Synchrotron Radiat.* **2008**, *15*, 185−190.
(8) Brintzinger, H. H.; Fischer, D.; Mulhaupt, R.; Rieger, B.; Waymouth, R. M. *Angew. Chem., Int. Ed. Engl.* **1995**, *34* (11), 1143−1170.
(9) Coates, G. W. *Chem. Rev.* **2000**, *100* (4), 1223−1252.
(10) Johnson, L. K.; Killian, C. M.; Brookhart, M. *J. Am. Chem. Soc.* **1995**, *117* (23), 6414−6415.
(11) Koutalas, G.; Iatrou, H.; Lohse, D. J.; Hadjichristidis, N. *Macromolecules* **2005**, *38* (12), 4996−5001.
(12) Fernyhough, C. M.; Young, R. N.; Poche, D.; Degroot, A. W.; Bosscher, F. *Macromolecules* **2001**, *34* (20), 7034−7041.
(13) Kumaraswamy, G.; Kornfield, J. A.; Yeh, F. J.; Hsiao, B. S. *Macromolecules* **2002**, *35* (5), 1762−1769.
(14) Kimata, S.; Sakurai, T.; Nozue, Y.; Kasahara, T.; Yamaguchi, N.; Karino, T.; Shibayama, M.; Kornfield, J. A. *Science* **2007**, *316* (5827), 1014−1017.
(15) Balzano, L.; Kukalyekar, N.; Rastogi, S.; Peters, G. W. M.; Chadwick, J. C. *Phys. Rev. Lett.* **2008**, *1* (4), xxxx.
(16) Janeschitz-Kriegl, H.; Ratajski, E.; Wippel, H. *Colloid Polym. Sci.* **1999**, *277* (2−3), 217−226.
(17) Andersen, P. G.; Carr, S. H. *Polym. Eng. Sci.* **1978**, *18* (3), 215−221.
(18) Haas, T. W.; Maxwell, B. *Polym. Eng. Sci.* **1969**, *9* (4), 225−&.
(19) Fujiyama, M.; Wakino, T.; Kawasaki, Y. *J. Appl. Polym. Sci.* **1988**, *35* (1), 29−49.
(20) Kantz, M. R.; Stigale, F. H.; Newman, H. D. *J. Appl. Polym. Sci.* **1972**, *16* (5), 1249−&.
(21) Trotignon, J. P.; Verdu, J. *J. Appl. Polym. Sci.* **1987**, *34* (1), 1−18.
(22) Liedauer, S.; Eder, G.; Janeschitzkriegl, H. *Int. Polym. Process.* **1995**, *10* (3), 243−250.
(23) Flory, P. J. *J. Chem. Phys.* **1947**, *15* (6), 397−408.
(24) Hill, M. J.; Keller, A. *J. Macromol. Sci., Phys.* **1969**, *B 3* (1), 153−&.
(25) Kumaraswamy, G.; Issaian, A. M.; Kornfield, J. A. *Macromolecules* **1999**, *32* (22), 7537−7547.
(26) Balzano, L.; Rastogi, S.; Peters, G. *Macromolecules* **2011**, *44* (8), 2926−2933.
(27) Seki, M.; Thurman, D. W.; Oberhauser, J. P.; Kornfield, J. A. *Macromolecules* **2002**, *35* (7), 2583−2594.
(28) Janeschitz-Kriegl, H.; Ratajski, E.; Stadlbauer, M. *Rheol. Acta* **2003**, *42* (4), 355−364.
(29) Balzano, L.; Cavallo, D.; Erp, T. B. V.; Ma, Z.; Housmans, J.-W.; Fernandez-Ballester, L.; Peters, G. W. M. *IOP Conf. Ser.: Mater. Sci. Eng.* **2010**, *14* (1), 012005.
(30) Janeschitz-Kriegl, H.; Ratajski, E. *Colloid Polym. Sci.* **2010**, *288* (16−17), 1525−1537.
(31) Kornfield, J. A.; Kumaraswamy, G.; Issaian, A. M. *Ind. Eng. Chem. Res.* **2002**, *41* (25), 6383−6392.
(32) Housmans, J. W.; Steenbakkers, R. J. A.; Roozemond, P. C.; Peters, G. W. M.; Meijer, H. E. H. *Macromolecules* **2009**, *42* (15), 5728−5740.
(33) Ogino, Y.; Fukushima, H.; Matsuba, G.; Takahashi, N.; Nishida, K.; Kanaya, T. *Polymer* **2006**, *47* (15), 5669−5677.
(34) Zhang, C.; Hu, H.; Wang, D.; Yan, S.; Han, C. C. *Polymer* **2005**, *46* (19), 8157−8161.
(35) Sherwood, C. H.; Price, F. P.; Stein, R. S. *J. Polym. Sci., Part C: Polym. Symp.* **1977**, *63*, 77−94.
(36) Jerschow, P.; JaneschitzKriegl, H. *Int. Polym. Process.* **1997**, *12* (1), 72−77.
(37) Vleeshouwers, S.; Meijer, H. E. H. *Rheol. Acta* **1996**, *35* (5), 391−399.
(38) Nogales, A.; Hsiao, B. S.; Somani, R. H.; Srinivas, S.; Tsou, A. H.; Balta-Calleja, F. J.; Ezquerra, T. A. *Polymer* **2001**, *42* (12), 5247−5256.
(39) Somani, R. H.; Yang, L.; Hsiao, B. S. *Polymer* **2006**, *47* (15), 5657−5668.
(40) Lagasse, R. R.; Maxwell, B. *Polym. Eng. Sci.* **1976**, *16* (3), 189−199.
(41) Keller, A.; Kolnaar, H. W. H. Flow-Induced Orientation and Structure Formation. In *Processing of Polymers*; Meijer, H. E. H., Ed.; Wiley-VCH: New York, 1997; Vol. *18*, pp 189−268.
(42) Duplay, C.; Monasse, B.; Haudin, J. M.; Costa, J. L. *J. Mater. Sci.* **2000**, *35* (24), 6093−6103.
(43) Graham, R. S.; Olmsted, P. D. *Phys. Rev. Lett.* **2009**, *103* (11), 4.
(44) Steenbakkers, R. J. A.; Peters, G. W. M. *J. Rheol.* **2011**, *55* (2), 401−433.
(45) van Meerveld, J.; Peters, G. W. M.; Hutter, M. *Rheol. Acta* **2004**, *44* (2), 119−134.
(46) Yang, L.; Somani, R. H.; Sics, I.; Hsiao, B. S.; Kolb, R.; Fruitwala, H.; Ong, C. *Macromolecules* **2004**, *37* (13), 4845−4859.
(47) Keum, J. K.; Zuo, F.; Hsiao, B. S. *Macromolecules* **2008**, *41* (13), 4766−4776.
(48) Heeley, E. L.; Fernyhough, C. M.; Graham, R. S.; Olmsted, P. D.; Inkson, N. J.; Embery, J.; Groves, D. J.; McLeish, T. C. B.; Morgovan, A. C.; Meneau, F.; Bras, W.; Ryan, A. J. *Macromolecules* **2006**, *39* (15), 5058−5071.
(49) Matsuba, G.; Sakamoto, S.; Ogino, Y.; Nishida, K.; Kanaya, T. *Macromolecules* **2007**, *40* (20), 7270−7275.
(50) Doufas, A. K.; Dairanieh, I. S.; McHugh, A. J. *J. Rheol.* **1999**, *43* (1), 85−109.
(51) Janeschitz-Kriegel, H.; Ratajski, E. *Polymer* **2005**, *46* (11), 3856−3870.
(52) Ballard, D. G. H.; Cheshire, P.; Longman, G. W.; Schelten, J. *Polymer* **1978**, *19* (4), 379−385.
(53) Hongladarom, K.; Burghardt, W. R.; Baek, S. G.; Cementwala, S.; Magda, J. J. *Macromolecules* **1993**, *26* (4), 772−784.
(54) Thurman, D. W. *Molecular Aspects of Flow-Induced Crystallization of Polypropylene*; California Institute of Technology: Pasadena, CA, 2005.
(55) Kumaraswamy, G.; Verma, R. K.; Kornfield, J. A.; Yeh, F. J.; Hsiao, B. S. *Macromolecules* **2004**, *37* (24), 9005−9017.
(56) Doi, M.; Edwards, S. F. *The Theory of Polymer Dynamics*; Oxford University Press: New York, 1986.
(57) Kumaraswamy, G.; Verma, R. K.; Issaian, A. M.; Wang, P.; Kornfield, J. A.; Yeh, F.; Hsiao, B. S.; Olley, R. H. *Polymer* **2000**, *41* (25), 8931−8940.
(58) White, H. M.; Bassett, D. C. *Polymer* **1997**, *38* (22), 5515−5520.
(59) Baert, J.; Van Puyvelde, P.; Langouche, F. *Macromolecules* **2006**, *39* (26), 9215−9222.
(60) Janimak, J. J.; Cheng, S. Z. D.; Giusti, P. A.; Hsieh, E. T. *Macromolecules* **1991**, *24* (9), 2253−2260.
(61) Eder, G.; Janeschitzkriegl, H.; Liedauer, S. *Prog. Polym. Sci.* **1990**, *15* (4), 629−714.
(62) Wang, M.; Hu, W.; Ma, Y.; Ma, Y.-q. *Macromolecules* **2005**, *38* (7), 2806−2812.
(63) Yan, T. Z.; Zhao, B. J.; Cong, Y. H.; Fang, Y. Y.; Cheng, S. W.; Li, L. B.; Pan, G. Q.; Wang, Z. J.; Li, X. H.; Bian, F. G. *Macromolecules* **2010**, *43* (2), 602−605.
(64) Somani, R. H.; Hsiao, B. S.; Nogales, A.; Srinivas, S.; Tsou, A. H.; Sics, I.; Balta-Calleja, F. J.; Ezquerra, T. A. *Macromolecules* **2000**, *33* (25), 9385−9394.

■ NOTE ADDED AFTER ASAP PUBLICATION

This article posted ASAP on August 1, 2012. Figures 8 and 12 have been revised. The correct version posted on August 2, 2012.